An Algorithm for Calculating Green's Functions of Planar, Circular Cylindrical, and Spherical Multilayer Substrates

Zvonimir Šipuš[1], Per-Simon Kildal[2], Robert Leijon[2] and Martin Johansson[3]
[1]Faculty of Electrical Engineering and Computing, University of Zagreb,
Unska 3, HR-10000 Zagreb, Croatia
[2] Department of Microwave Technology, Chalmers University of Technology,
SE-412 96 Göteborg, Sweden
[3]Ericsson Microwave Systems AB, SE-431 84 Mölndal, Sweden

Abstract— **We introduce an algorithm for calculating spectral domain Green's functions of planar, circular cylindrical and spherical multilayer structures. The three spectral domain problems are interpreted as multilayer spatial domain problems with electromagnetic sources in the forms of current sheets, tubes and shells, respectively, and with harmonic spatial variation. The algorithm, which is the same for all three geometries, is based on dividing these three field problems into appropriate subproblems by using equivalence, and on determining the tangential field components at the interfaces between the layers of the structure. The algorithm is implemented into three versions of a Fortran routine called G1DMULT, one version for each geometry. The only difference between the three versions is in two subroutines which calculate the fields due to harmonic current sheets, tubes and shells, respectively, located in an infinite homogeneous material. We have tested the routine by calculating the properties of microstrip patch antennas and periodic structures.**

I. Introduction

ANTENNAS on planar or curved ground planes or substrates find many applications in communication and radar systems. Microstrip patch antennas and arrays are often used because of their thin profile, light weight and low cost, and because they can be made to conform with a curved structure. Periodic elements on substrates can be used as frequency or polarization selective subreflectors in reflector antenna systems or as radomes. When the curvature of the substrate is small, such antennas can be analyzed by assuming it to be planar. If this is not the case, more precise methods must be used.

The purpose of this paper is to introduce a general numerical algorithm G1DMULT for computing Green's functions in the spectral domain. The algorithm is based on the ideas in [1] and has the advantage of analytic simplicity. It is applicable to planar, circular cylindrical and spherical multilayer structures with an arbitrary number of material layers. The knowledge of the Green's functions of such multilayer structures is needed when analyzing e.g. microstrip antennas [2] and frequency selective surfaces [3] by applying the integral equation approach and the moment method. We also describe how layers with corrugations and strips are included in G1DMULT, provided that their periods are small compared to the wavelength. Another advantage of the layout of G1DMULT is that it can be reused even for two-dimensional structures, such as multiregion cylindrical structures of arbitrary cross-section.

The spectral Green's functions for planar and circular cylindrical multilayer structures have been studied by a lot of authors, e.g. [4]-[10]. In one of the methods the z-component of the electromagnetic field (or vector potential) is determined by fulfilling the boundary conditions [4]-[8], and from this the other components are calculated. For multilayer structures this method leads to finding the reflection and transmission coefficients of waves propagating inside the structure [6]-[8]. In the second method, called the impedance method, the problem is reduced to two one-dimensional transmission line problems, one for TE_z and one for TM_z case. In the multilayer case the method leads to solving the transmission line problem with a lot of transmission line pieces by using the reflection and transmission coefficients at the layer interfaces [10], in the same way as for the former method. Our approach has similarities to the first of these approaches. The main difference is that we determine the transverse components of the electromagnetic field at the boundaries between the layers by solving a system of linear equations. The number of equations is four times the number of material interfaces. This is done by dividing the problem into equivalent subproblems, one for each layer in the multilayer structure.

We have previously presented the general methodology and common terminology by which planar, cylindrical and spherical multilayer structures can be analyzed and described [1]. In all three cases the problem is transformed into the spectral domain resulting in a one-dimensional (1D) problem to solve. We refer to this approach as analysis by using a spectrum of one-dimensional solutions (S1DS). The basis of the approach

1054-4887 © 1998 ACES

is to interpret the spectral domain problem as a spatial domain problem which consists of the multilayer structure and sources in the form of current sheets, tubes and shells in the planar, cylindrical and spherical geometries, respectively. The present paper describes how the methodology has been reduced to an algorithm and implemented in a Fortran subroutine G1DMULT for calculating the Green's functions of all three types of multilayer structures (G1DMULT = Green's functions of 1D MULTilayer structures).

II. Description of G1DMULT algorithm for planar substrates

The algorithm for the planar case is illustrated on the left in Fig. 1. The same procedure is used for the circular cylindrical and spherical cases and the differences will be described later. The original 3D problem (Fig. 1.a) is transformed to the spectral domain (Fig. 1.b) by performing the Fourier transformation

$$\tilde{\mathbf{J}}(k_x,k_y,z)=\int_{-\infty}^{\infty}\int_{-\infty}^{\infty}\mathbf{J}(x,y,z)e^{jk_x x}e^{jk_y y}\,dxdy\ , \tag{1}$$

$$\mathbf{J}(x,y,z)=\frac{1}{4\pi^2}\int_{-\infty}^{\infty}\int_{-\infty}^{\infty}\tilde{\mathbf{J}}(k_x,k_y,z)e^{-jk_x x}e^{-jk_y y}\,dk_x dk_y\ . \tag{2}$$

The sources in the spectral domain are interpreted in space as a spectrum of current sheets of the form $\tilde{\mathbf{J}}(k_x,k_y)e^{-jk_x x}e^{-jk_y y}$ and $\tilde{\mathbf{M}}(k_x,k_y)e^{-jk_x x}e^{-jk_y y}$ which extends infinitely in x- and y-direction, in the same way as the structure. Each current sheet excites two plane waves, one propagating upwards away from the sheet and another downwards away from it (see Appendix). The presence of the multilayer structure will cause a number of transmitted and reflected waves in each layer, with propagation constants equal to k_x, k_y and $k_{zn}=\pm\sqrt{k_n^2-k_x^2-k_y^2}$ in the x, y and z directions, where the index n denotes the nth layer, $k_n=k_0\sqrt{\epsilon_{rn}\mu_{rn}}$ is the wave impedance of the nth layer, ϵ_{rn} and μ_{rn} are the relative permittivity and permeability of the nth layer, and $k_0=2\pi/\lambda_0$ is the free-space wave number. Notice that all the waves have the same propagation constant in the x and y directions for all layers, which is a consequence of the boundary conditions. Therefore, the problem of determining the Green's functions is a harmonic 1D problem in space with known harmonic variation in x and y directions and unknown variation in z direction. We have to solve this 1D problem for a spectrum of k_x and k_y, and in order to find the 3D solution we must combine the solutions by a summation over the complete k_x and k_y spectrum, corresponding to an inverse Fourier transformation.

The algorithm G1DMULT is based on subdividing the spatial harmonic problem into one equivalent problem per layer (Figs. 1.c and 1.d), where the field in each region is formulated as the field radiated by equivalent currents at the layer boundaries. For example, the E-field in the layer j is expressed as

$$\begin{aligned}\tilde{\mathbf{E}}_j=&\tilde{\mathbf{G}}_{EJ}^{homo}\tilde{\mathbf{J}}_{j-1}+\tilde{\mathbf{G}}_{EJ}^{homo}\tilde{\mathbf{J}}_j+\tilde{\mathbf{G}}_{EM}^{homo}\tilde{\mathbf{M}}_{j-1}\\&+\tilde{\mathbf{G}}_{EM}^{homo}\tilde{\mathbf{M}}_j+\tilde{\mathbf{G}}_{EJ}^{homo}\tilde{\mathbf{J}}_j^{exci}+\tilde{\mathbf{G}}_{EM}^{homo}\tilde{\mathbf{M}}_j^{exci}\end{aligned} \tag{3}$$

where $\tilde{\mathbf{J}}_j$ and $\tilde{\mathbf{M}}_j$ are equivalent electric and magnetic current sheets at boundary j, $\tilde{\mathbf{J}}_j^{exci}$ and $\tilde{\mathbf{M}}_j^{exci}$ are excitation electric and magnetic currents in layer j (if any), and $\tilde{\mathbf{G}}^{homo}$ is the Green's function of the homogeneous problem (see Appendix). By using $\tilde{\mathbf{J}}_j=\pm\hat{z}\times\tilde{\mathbf{H}}_j$ and $\tilde{\mathbf{M}}_j=\mp\hat{z}\times\tilde{\mathbf{E}}_j$ eq. (3) can be expressed in terms of the unknown tangential E- and H-fields $\mathbf{E}_j$ and $\mathbf{H}_j$ at the boundary j between layers j and $j+1$ and known excitation currents. The boundary conditions that the tangential E- and H- fields are continuous at the layer boundaries give 4 linear equations per boundary. The tangential E- and H-fields are evaluated by solving the system of $4(N_{layer}-1)$ equations with $4(N_{layer}-1)$ unknowns, where N_{layer} is the number of layers in the multilayer structure. After they have been determined, the total E- and H-fields at any desired z-location can be found by using the equivalent problem in Fig. 1.d.

The core of G1DMULT is two subroutines G1DJ and G1DM for calculation of the fields radiated by electric and magnetic current sheets in an infinite homogeneous material (Fig. 1.e). The used formulas are given in the Appendix. The rest of the Fortran G1DMULT routine is simply a programming of the logical layout of the algorithm.

The input variables of the planar version of G1DMULT are:

- the spectral variables k_x, k_y which can be generally complex,
- the parameters describing the multilayer structure: the z-coordinates of the interfaces between the dielectric layers, and the complex wave impedances and wave numbers of all the layers,
- the z-coordinates and amplitudes of the current sheet sources $\tilde{\mathbf{J}}^{exci}$ and $\tilde{\mathbf{M}}^{exci}$, which can have x-, y- and z-components.
- the z-coordinates of the desired points at which the output fields are calculated.

The routine calculates the values of the x, y and z components of the E- and H-fields at the desired z-locations as a result of the excitation currents. The spectral domain Green's function is calculated by G1DMULT by choosing unit amplitude of the excitation current sheet, and evaluating the fields as a function of k_x and k_y.

Fig. 2 shows the flow chart of the routine G1DMULT. The program consists of three loops inside each other.

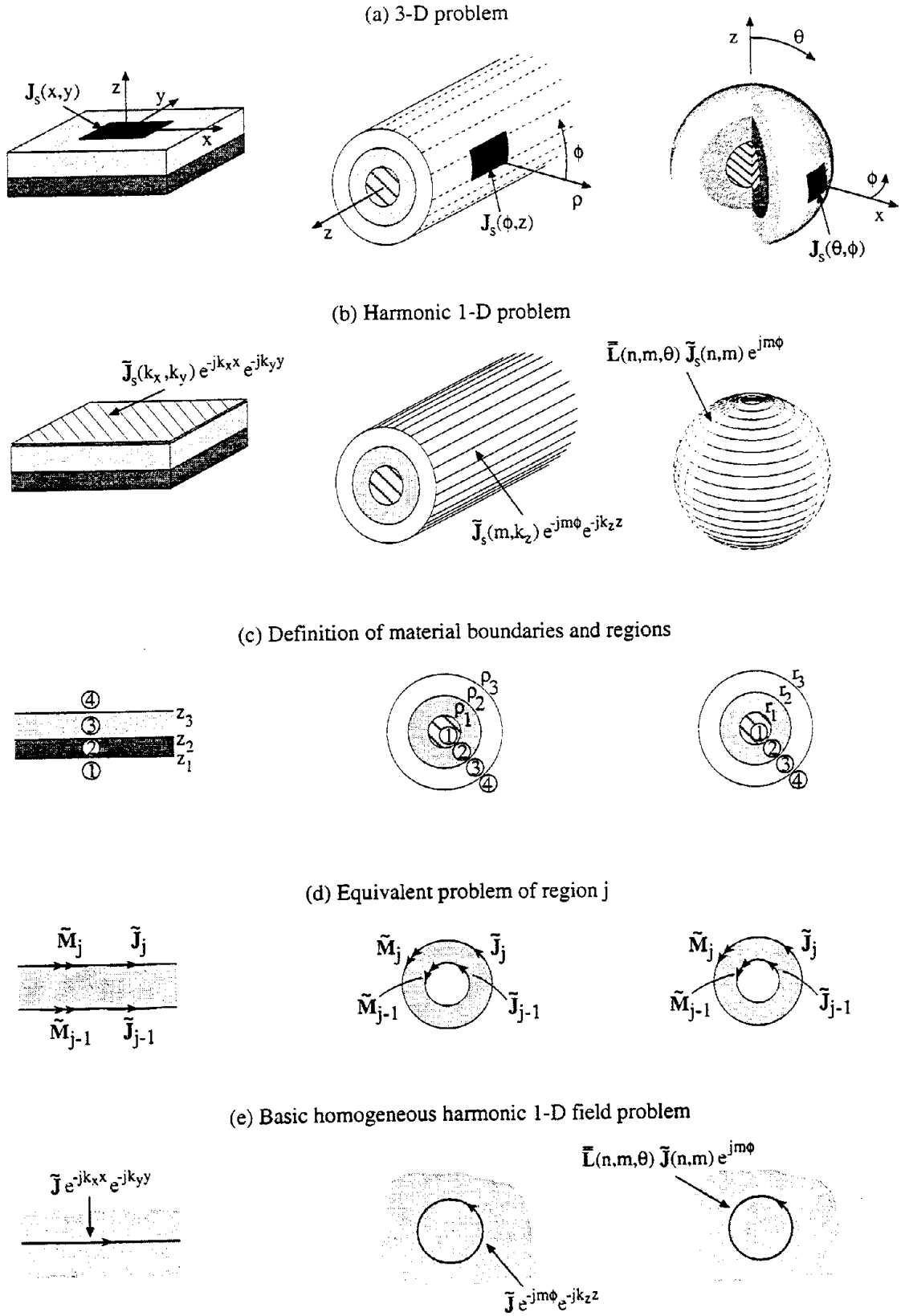

Figure 1. Structuring of a 3D field problem with a planar layered structure into a harmonic 1D problem and its subproblems. The G1DMULT subroutine solves the harmonic 1D problem.

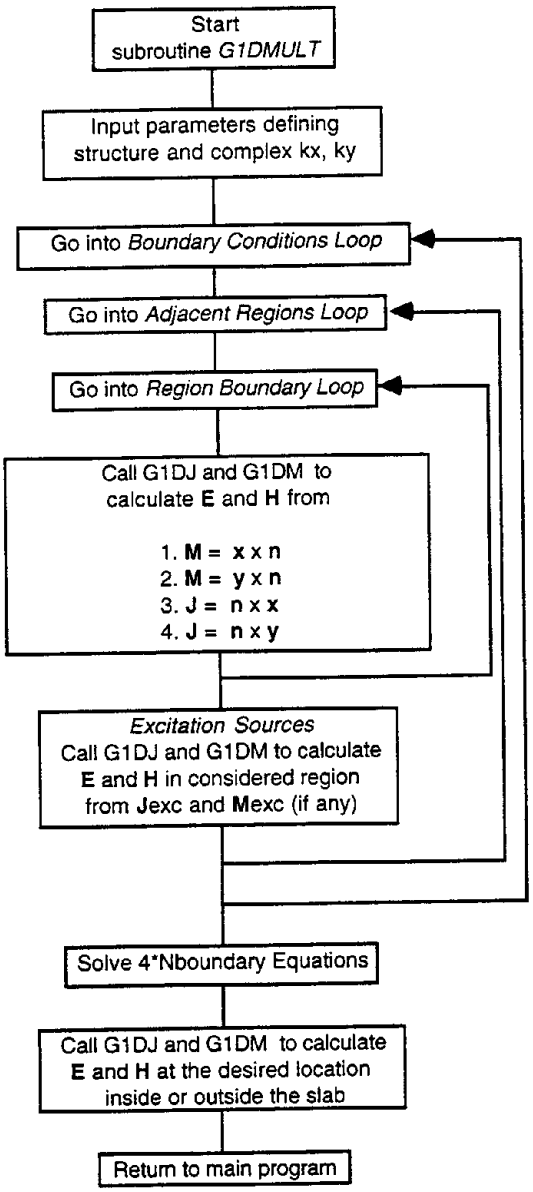

Fig. 2. Flow chart of routine G1DMULT for solving 1D field problem.

The first loop is taken over all layer boundaries j, $1 \leq j \leq N_{layer} - 1$, referred to as the boundary condition loop, in order to generate the $4(N_{layer} - 1)$ equations to determine the two components of both the tangential E- and H-fields at each boundary. The second loop is referred to as the adjacent region loop. This loop selects the regions below and above each boundary j. The intention is to consider the two components of both the tangential E- and H-fields in both regions, and to set up the four equations to make them equal at the boundary j. Any of these field components are given by a sum of contributions from the equivalent currents due to the tangential E- and H-fields at the both boundaries of the considered region. Therefore, the inner third loop goes over the lower and upper boundary of the considered region below or above the boundary j. This third loop is referred to as the region boundary loop. The tangential E- and H-fields are calculated by using the two core subroutines G1DJ and G1DM (Fig. 1.e). At the end of G1DMULT the system of $4(N_{layer} - 1)$ equations is solved by using LU decomposition for banded matrices, and then the output E- and H-fields are evaluated at the desired z-locations along the z-axis.

III. Description of G1DMULT Algorithm for Circular Cylindrical and Spherical Substrates

Cylindrical substrates: In the cylindrical case, we use the cylindrical-Fourier transformation

$$\tilde{\mathbf{J}}(\rho, m, k_z) = \int_{-\pi}^{\pi} \int_{-\infty}^{\infty} \mathbf{J}(\rho, \phi, z) e^{jm\phi} e^{jk_z z} dz d\phi \ , \tag{4}$$

$$\mathbf{J}(\rho, \phi, z) = \frac{1}{4\pi^2} \sum_{m=-\infty}^{\infty} \int_{-\infty}^{\infty} \tilde{\mathbf{J}}(\rho, m, k_z) e^{-jm\phi} e^{-jk_z z} dk_z \ . \tag{5}$$

In this case we can interpret the spectral sources as current tubes in space with harmonic variation in ϕ and z. The spectral variables are m and k_z, and the structure varies with ρ. Similarly to the planar case k_z is generally complex, while m is an integer. After the Fourier transformation we have a 1D problem in ρ. The explanation of the routine is the same as for the planar case, with planes and sheets changed to tubes (see Fig. 1). The only difference compared to the planar case is in the two core subroutines G1DJ and G1DM which calculate the value of the electromagnetic field due to electric and magnetic current tubes (see Appendix and Fig. 1.e).

The expressions for the electromagnetic field due to the current tube contain Bessel and Hankel functions (eqs. (17)-(24)). To improve the numerical efficiency we tabulate their values for the arguments needed in the G1DMULT routine, i.e., for each k_z we make a table of the values of the Bessel and Hankel functions for all m and for all arguments $\sqrt{k_n^2 - k_z^2}\rho$ corresponding to the ρ-coordinates of the boundaries and of the source and observation points (see eqs. (17)-(24)). The reason for doing this is that an mth order Bessel/Hankel function in most commercial libraries is calculated in the recursive way by evaluating all Bessel/Hankel functions from 0th to mth order, which is not very time efficient unless storing and reusing intermediate results like we do.

We also noticed numerical problems when the argument of the Bessel and Hankel functions is large and imaginary ($\mathrm{Im}(arg) \leq 0$ due to the chosen branch cut of

the function $\sqrt{k_n^2 - k_z^2}$ [7]). This happens e.g. when performing the inverse Fourier transformation for calculating the input impedance of cylindrical patch antennas. If we consider the expressions in eqs. (17)-(24), we see that they contain products of the Bessel and Hankel function. The arguments of Bessel and Hankel functions in eqs. (17)-(24) are almost the same for thin substrates (i.e., when the radial distance between the observation and source point is small), which is usually the case in practice. Furthermore, the asymptotic behavior of Bessel and Hankel functions for large negative imaginary argument is $J_m(-jv) \sim e^v$ and $H_m^{(2)}(-jv) \sim e^{-v}$ [11]. Therefore, in order to avoid numerical difficulties, we evaluate the Bessel and Hankel functions with extracted exponential parts, since the Bessel and Hankel functions have opposite exponential behavior for large negative imaginary arguments. Thereby, we avoid the numerical problems.

Spherical substrates. In the spherical case we again analyze the problem in the spectral domain. We choose the vector Legendre transformation defined in [12] and [13], i.e.,

$$\tilde{\mathbf{J}}(r,n,m) = \begin{bmatrix} \tilde{J}_r \\ \tilde{J}_\theta \\ \tilde{J}_\phi \end{bmatrix} = \frac{1}{2\pi S(n,m)} \int_{-\pi}^{\pi} \int_{0}^{\pi} \bar{\bar{\mathbf{L}}}(n,m,\theta)\mathbf{J}(r,\theta,\phi)\sin\theta e^{-jm\phi} d\theta d\phi \tag{6}$$

$$\mathbf{J}(r,\theta,\phi) = \begin{bmatrix} J_r \\ J_\theta \\ J_\phi \end{bmatrix} = \sum_{m=-\infty}^{\infty} \sum_{n=m}^{\infty} \bar{\bar{\mathbf{L}}}(n,m,\theta)\tilde{\mathbf{J}}(r,n,m)e^{jm\phi} \tag{7}$$

$$\bar{\bar{\mathbf{L}}}(n,m,\theta) = \begin{bmatrix} L_{rr} & 0 & 0 \\ 0 & L_{\theta\theta} & L_{\theta\phi} \\ 0 & L_{\phi\theta} & L_{\phi\phi} \end{bmatrix}$$

$$\begin{aligned} L_{rr} &= P_n^{|m|}(\cos\theta)\sqrt{n(n+1)} \\ L_{\theta\theta} &= \frac{\partial P_n^{|m|}(\cos\theta)}{\partial\theta} \\ L_{\theta\phi} &= -\frac{jmP_n^{|m|}(\cos\theta)}{\sin\theta} \\ L_{\phi\theta} &= \frac{jmP_n^{|m|}(\cos\theta)}{\sin\theta} \\ L_{\phi\phi} &= \frac{\partial P_n^{|m|}(\cos\theta)}{\partial\theta} \end{aligned} \tag{8}$$

$$S(n,m) = \frac{2n(n+1)(n+|m|)!}{(2n+1)(n-|m|)!}, \tag{9}$$

where $P_n^{|m|}(\cos\theta)$ are the associated Legendre functions of the first kind. In this case we interpret the sources as spherical current shells with harmonic variations in θ and ϕ (the variation in θ-direction is actually a quasi-harmonic Legendre-type variation). The spectral variables are n and m (both are integers), and the structure varies with r. Note that each spectral θ or ϕ components is obtained from both the spatial θ and ϕ components. In this case a spatial interpretation of $\tilde{J}_\theta$ (or $\tilde{J}_\phi$) as a harmonic current shell with only θ-directed (or ϕ-directed) currents is not correct since there are also spatial ϕ-components (or θ-components) of the current present. The explanation of the routine is the same as for the planar case, with planes and sheets changed to spheres and shells (see Fig. 1). The two core subroutines G1DJ and G1DM now calculate the electromagnetic fields due to an electric and magnetic current shell in an homogeneous region (see the Appendix; the details of the spherical case can be found in [13]). These two subroutines are the only part which makes G1DMULT for the spherical case different from the planar and cylindrical cases. The rest of the routine is the same for all three geometries. The Legendre polynomials are not needed within G1DMULT since they occur in the transformation from the spatial to the spectral domain and G1DMULT is a spectral domain routine.

IV. Implementation of Asymptotic Corrugation and Strip Boundary Conditions in G1DMULT

Previously, multilayer planar/cylindrical/spherical structures have been analyzed by writing the field quantities within each region as the superposition of a forward and a backward traveling wave, and solving for the unknown coefficients of these waves by enforcing the continuity of the tangential field components at each interface [8]. Although in our approach we also consider traveling waves, the way of determining the tangential field components at each interface is different. We calculate the transverse field components simultaneously in contrast with computing the reflection and transmission coefficients in a recursive way.

The advantage of our algorithm is that it has a reusable structure because planar, cylindrical and spherical problems can be analyzed with a change of only the two core subroutines G1DJ and G1DM. In a similar way G1DMULT can also be extended to analyze two-dimensional (2D) structures, such as multilayer cylindrical structures of arbitrary cross-section shape. All subproblems have current sources and Green's functions, so it is easy to formulate the solution. The particular advantage of our approach is that the algorithm can be easily modified. For example, we have built a corrugated metal layer into the algorithm by using impedance

boundary conditions which depend on the spectral variables, k_x and k_y in the planar case and $e^{jn\phi}$ and k_z in the cylindrical case. The impedance boundary conditions are implemented into the routine by coupling the unknown tangential E- and H-fields at the appropriate boundary. This coupling results in multiplying one column of the matrix, whose elements are the coefficients of the $4(N_{layer}-1)$ unknowns in the system of $4(N_{layer}-1)$ equations, by the impedance boundary condition, and adding the multiplied column to the column belonging to the coupled field component. By doing this we reduce the dimensionality of the problem by one.

We can model arbitrary corrugated surfaces by using generalized impedance boundary conditions referred to as the asymptotic corrugation boundary conditions (ACBC) [14], [15], which are asymptotically valid when the corrugation period approaches zero. The ACBC simplify the analysis considerably. The ACBC states that the electric field parallel with the corrugations is zero (since the period of the corrugations is small compared with the wavelength and the field is shorted by the ridges between the grooves), and that the ratio of the tangential electric field component (which is orthogonal to the direction of the corrugation) and the tangential magnetic field component (which is parallel with the corrugations) is determined by a two-dimensional solution of the field problem inside each corrugation obtained by enforcing no field variation in the direction orthogonal to the corrugation walls. For canonical planar and circular cylindrical geometries the ACBC corresponds to using the impedance boundary conditions in the spectral domain. Assuming planar y-directed corrugations, the spectral impedance boundary conditions at the top of the corrugations are

$$\tilde{Z}_{xy} = \frac{\tilde{E}_x}{\tilde{H}_y} = -j\eta\frac{w}{p}\frac{k}{\sqrt{k^2-k_y^2}}\tan(d\sqrt{k^2-k_y^2})$$
$$\tilde{Z}_{yx} = \frac{\tilde{E}_y}{\tilde{H}_x} = 0\,, \tag{10}$$

where d is the depth of the corrugations, w is the width of the grooves, p is the period of the corrugations, and k and η are the wave number and the wave impedance of the medium inside the corrugations. The $\tilde{Z}_{xy}$ term is calculated by considering the corrugations as parallel plate waveguides which are short-circuited at the bottom [16]. In the cylindrical case we have for ϕ-directed corrugations

$$\tilde{Z}_{z\phi} = \frac{\tilde{E}_z}{\tilde{H}_\phi} = j\eta\frac{w}{p}\frac{J_m(k\rho_t)H_m^{(2)}(k\rho_b) - J_m(k\rho_b)H_m^{(2)}(k\rho_t)}{J_m'(k\rho_t)H_m^{(2)}(k\rho_b) - J_m(k\rho_b)H_m^{(2)'}(k\rho_t)}$$
$$\tilde{Z}_{\phi z} = \frac{\tilde{E}_\phi}{\tilde{H}_z} = 0\,, \tag{11}$$

where ρ_b and ρ_t are the values of the radial coordinate ρ at the bottom and the top of corrugations. For z-directed wedge-type corrugations we have

$$\tilde{Z}_{\phi z} = \frac{\tilde{E}_\phi}{\tilde{H}_z} = j\eta\frac{w}{p}\frac{J_0'(k\rho_t)H_0^{(2)'}(k\rho_b) - J_0'(k\rho_b)H_0^{(2)'}(k\rho_t)}{J_0(k\rho_t)H_0^{(2)'}(k\rho_b) - J_0'(k\rho_b)H_0^{(2)}(k\rho_t)}$$
$$\tilde{Z}_{z\phi} = \frac{\tilde{E}_z}{\tilde{H}_\phi} = 0\,. \tag{12}$$

For determining $\tilde{Z}_{z\phi}$ and $\tilde{Z}_{\phi z}$ we have considered propagation inside radial parallel-plate and wedge waveguides, respectively [16].

Another advantage of the algorithm is that strip gratings on one or more material layers can be included in the calculations by using the asymptotic strip boundary condition (ASBC) [14], [17]. This is asymptotically valid when the strip period approaches zero. Rigorously strips inside the multilayer structure can be analyzed by expanding the electromagnetic field in Floquet modes, which is a laborious procedure if the source excites a spectrum of plane waves, such as a Hertz dipole. In short, the ASBC state that the electric field parallel to the strips is zero, and that the electric field normal to the strips and the magnetic field parallel to strips are continuous through the strip layer. For example, for ϕ-directed strips we have

$$E_\phi^+ = 0\,, \qquad E_\phi^- = 0\,,$$
$$E_z^+ = E_z^-, \qquad H_\phi^+ = H_\phi^-\,, \tag{13}$$

where superscripts $-$ and $+$ stand for the lower and upper side of the strips. This boundary condition has been easily implemented into the algorithm by defining a layer of zero thickness which contains the strips, and by forcing the component of the electric field which is parallel to the strips to be zero at both boundaries of this layer. The ACBC and ASBC have not yet been implemented into the spherical version of G1DMULT.

V. Numerical results

G1DMULT has been tested by comparing the output values with the values of analytically derived Green's functions for single- and double-layered dielectric substrates [9], for strip-loaded dielectric slabs [18], and for corrugated surfaces [18]. Additional tests have been performed by adding several artificial layers inside or outside the substrate, all having the same relative permittivity and permeability as the substrate or the exterior region, respectively. In all calculated cases the relative error, compared to the calculations of the analytical Green's functions, was smaller than 10^{-10}.

We have also compared the computational time needed for using G1DMULT with analytically derived Green's

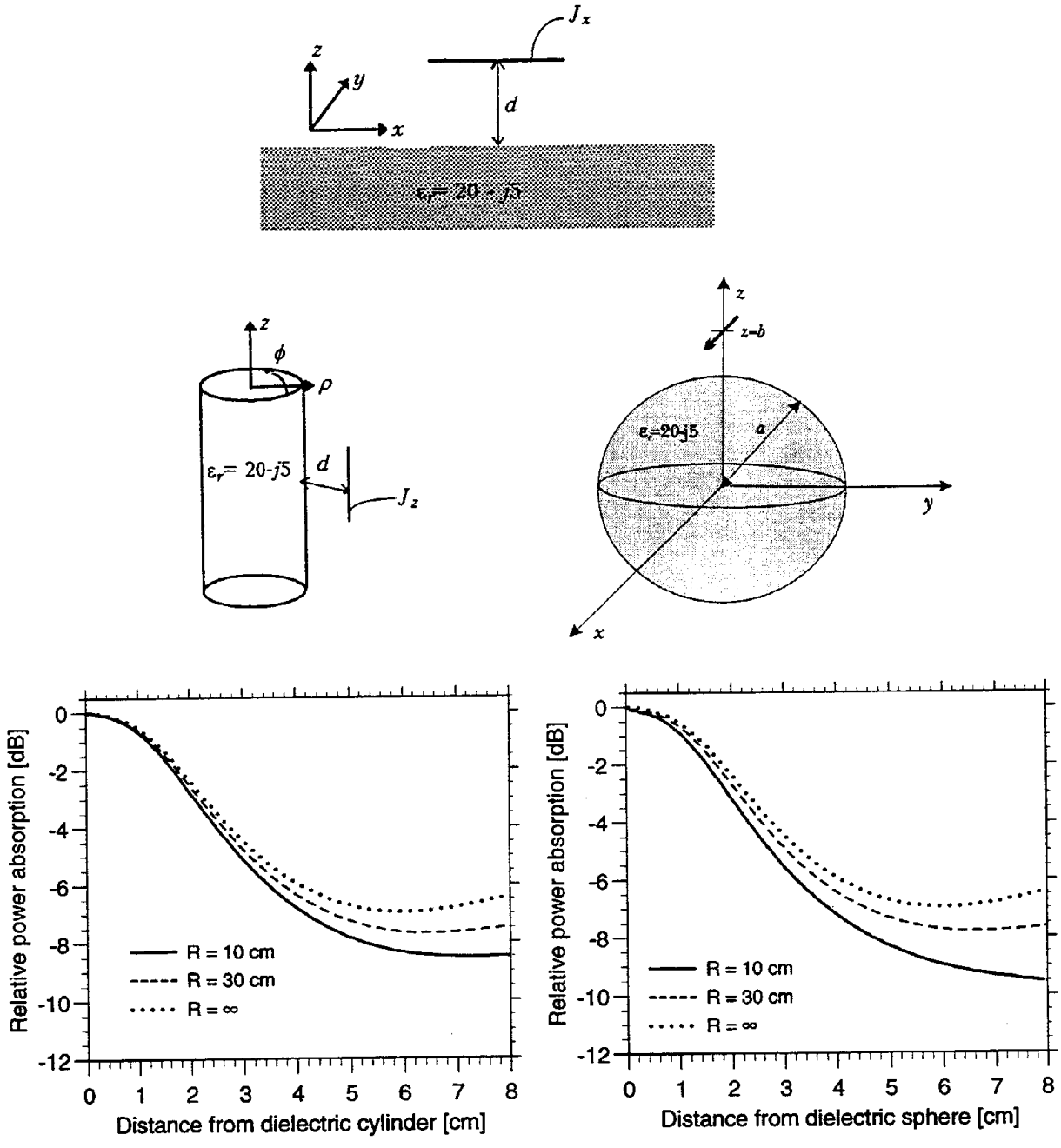

Fig. 3. Relative absorbed power of a short dipole near a dielectric half-space, cylinder and sphere. The radius R of the dielectric cylinder and sphere is parameter (for the dielectric half-space $R = \infty$). Frequency is 1.8 GHz.

function. Single-layer and double-layer planar geometries as well as a single-layered cylindrical geometry were considered. The analytic expressions are between 15 and 35 times faster than G1DMULT, depending on the geometry. Thus the disadvantage of G1DMULT is it's larger computational time. The advantage is, as mentioned before, that G1DMULT easily can be used for any number of material layers and for any location of the excitation. The analytic formulas are only of usable forms for a small number of layers, and a small change in the topology of the problem, such as moving the source to another layer, requires a new analytic expression for the Green's function.

G1DMULT has been implemented in different main programs for calculating the input impedance and radiation pattern from microstrip dipoles and patches, and for calculating scattering from corrugated and strip-loaded cylinders. The results have been tested against measured results and results calculated by other methods.

Dipole radiation: We have considered a short dipole radiating in the presence of a dielectric half-space, a cylinder and a sphere (Fig. 3), which can be looked upon as a simple model of a mobile phone antenna in the presence of the human head. The relative permittivity is $\epsilon_r = 20 - j5$ which resembles a mixture of human tissues and bones. The frequency is $f = 1.8\ GHz$. The value of interest is the relative absorbed power which is defined as the ratio between the absorbed power and the total radiated power. The radius of the cylinder/sphere and the height of the dipole over the half-space/cylinder/sphere are taken as parameters. The absorbed power is calculated by integrating the Poynting vector $\mathbf{E} \times \mathbf{H}^*$ over the dielectric interface, and by using Parseval's theorem to transform the integrand to the spectral domain. The results in Fig. 3 show that by enlarging the radius of the cylinder or sphere, the relative absorbed power approaches the planar case, i.e., radiation in the presence of a dielectric half-space, which is a good test for our program. Furthermore, we have compared the results of our program with analytic results for some canonical problems [13]. In this example, which makes use of the Poynting vector, it was not possible to change the contour of integration in order to avoid the poles of the Green's function because the complex conjugate of the magnetic field $\tilde{\mathbf{H}}^*$ is not an analytic function (the arguments k_x and k_y of the function $\tilde{\mathbf{H}}$ are complex). We could have avoided this problem if we had considered the magnetic field $\mathbf{H}$ as a complex function of the real arguments k_x and k_y, and had performed the complex conjugate. Thereafter, we could have extended the function to the complex arguments k_x and k_y and deformed the contour of integration. However, we cannot use this approach as we do not evaluate the magnetic field analytically.

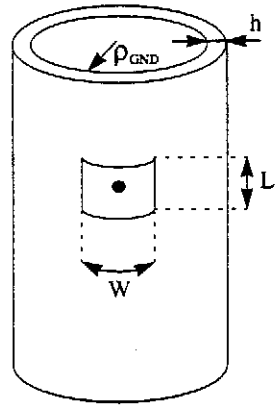

Fig. 4. Cylindrical patch antenna

Patch impedance, cylindrical case: We considered a cylindrical patch wrapped around a metal cylinder with a dielectric substrate, as reported in [19] (see Fig. 4). We built G1DMULT into a moment method program for determining the radiation pattern and input impedance of a cylindrical-rectangular patch. We modelled the patch current by 7 entire-domain basis functions. The patch is excited by a probe, so we modelled the probe as a constant current distribution. By using symmetries we halved the summation and integration in the inverse Fourier transformation, i.e. the sum and integral in eq. (5) were taken from 0 to ∞. To avoid surface wave poles in the k_z integral, the integration contour was deformed appropriately in the first quadrant of the complex plane [20]. The convergence of the ϕ modes and the length of k_z integration were checked for every calculated antenna (80 ϕ modes and $250k_0$ as a upper limit of the k_z integral were taken to get accurate approximation of the infinite summation and integration). Table 1 shows the comparison between the measured and calculated resonance frequencies and the resistances of the three coaxially fed cylindrical-rectangular patch antennas. The resonance frequency is defined as the frequency where the real part of the input impedance has a maximum (at the resonant frequency the imaginary part is positive due to the inductive self-impedance of the coax probe). The antennas are produced on a dielectric substrate with $\epsilon_r = 2.32$ and thickness 0.08 cm, and they are excited in the TM_{01} mode (i.e. the patch current is mainly z-oriented). The radius of the ground plane is $\rho_{GND} = 5$ cm. The lengths and widths of the patches are: $L_1 = L_2 = 6.5$ cm, $L_3 = 3$ cm, $W_1 = 8$ cm, $W_2 = 11$ cm, $W_3 = 4$ cm. More details about the measurements can be found in [19]. The agreement between the measured and calculated results is good. We have also tested the program for the case when the patch antenna is printed on a two-layer substrate, and the results can be found in [21].

antenna	1	2	3
f_{res} meas.	1.499 GHz	1.497 GHz	3.166 GHz
f_{res} cal.	1.498 GHz	1.495 GHz	3.199 GHz
R_{in} meas.	52.5 Ω	36.7 Ω	119.1 Ω
R_{in} cal.	63.0 Ω	41.6 Ω	114.0 Ω

TABLE I
COMPARISON OF RESONANCE FREQUENCIES AND RESONANT RESISTANCES FOR CYLINDRICAL-RECTANGULAR MICROSTRIP ANTENNA. THE MEASURED RESULTS ARE FROM [20].

Scattering from circumferential strips and corrugations: In order to evaluate the accuracy of the ASBC and ACBC, we have also developed a program for analyzing a grid of circumferential strips in a multilayer cylindrical structure by using a rigorous Floquet-mode expansion/moment method approach. This program also uses the G1DMULT subroutine for evaluation of the Green's functions. The two approaches are compared in Fig. 5 for normal incidence. The shown scattered fields are normalized to $E_i\sqrt{2j/\pi k\rho}\ \exp(-jk\rho)$. The dielectric cylinder has $\epsilon_r = 2.1$, radius $\rho = 1.27$ cm, and the strips are located at the dielectric-air interface. The frequency is 10 GHz, and the period and width of the strips are $p = 0.8$ cm and $w = 0.3$ cm, i.e $0.27\lambda_0$ and $0.1\lambda_0$, respectively. In the rigorous Floquet-modes approach four basis functions are used in the moment method procedure, which is sufficient for this strip width [22]. Results show that the ASBC give accurate results for the periodicities and widths of strips which are used in practice. For corrugations the comparison of the ACBC results with the mode-matching result is shown in Fig. 6. The parameters of the corrugations are $\epsilon_r = 4.8$, the inner and outer radius $\rho_b = 0.38$ cm and $\rho_t = 0.6$ cm, and the width of the grooves and the period of the corrugations are $w = 0.3$ cm and $p = 0.4$ cm. The equivalent blockage width is defined in [23] and is a complex parameter representing the amplitude and phase of the forward scattered field. The results obtained by the mode-matching are taken from [24].

VI. CONCLUSION

We have developed a routine called G1DMULT for calculating the Green's functions of planar, circular cylindrical and spherical multilayer structures in the spectral domain. The routine has the same layout for all three cases. The only difference is in the subroutines which compute the electromagnetic field in the homogeneous

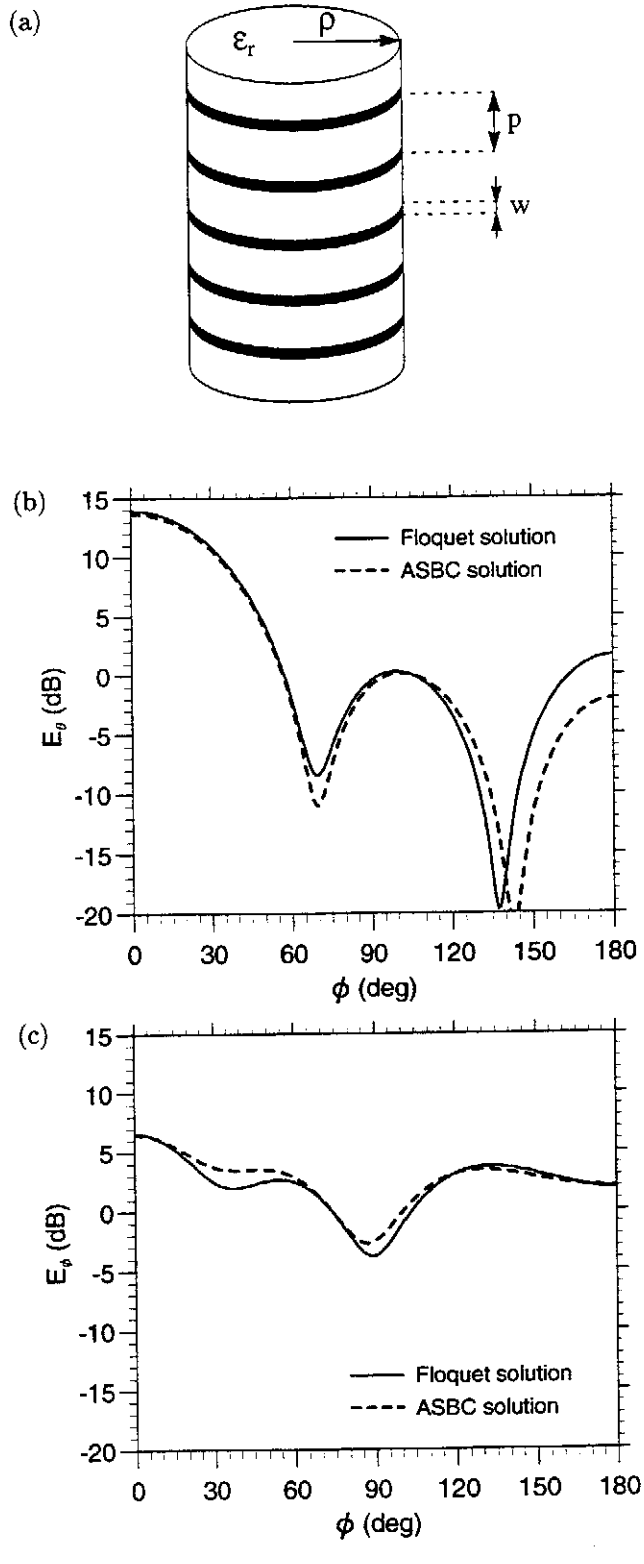

Fig. 5. Scattered field from a dielectric cylinder loaded with periodic circumferential strips. (a) geometry, (b) TM_z polarized normal incident field, (c) TE_z polarized normal incident field.

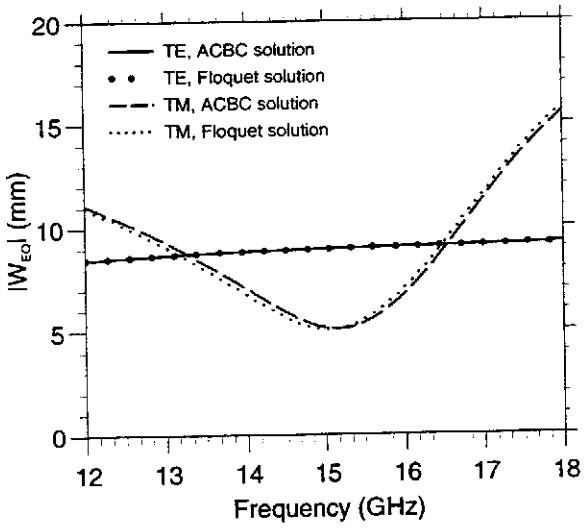

Fig. 6. Amplitude of equivalent blockage width of a corrugated cylinder.

space radiated by a current sheet, tube and shell, respectively. The advantage of the algorithm upon which G1DMULT is based is its simplicity. For example, it was easy to implement anisotropic spectral impedance boundary conditions, by which we have analyzed corrugations and metal strips inside the multilayer structure.

We have also used G1DMULT as a subroutine in moment method programs for calculating input impedance of microstrip patches and dipoles, and properties of periodic structures.

VII. Appendix

In this appendix we will give the formulas for the E- and H-fields radiated by the electric current sheet/tube/shell in the homogeneous space. The fields radiated by the magnetic current sources can be easily determined by the concept of duality [16].

Planar case. The electromagnetic field radiated by an electric current sheet located in the plane $z = 0$ in the homogeneous space is given by

$$\tilde{\mathbf{E}}(k_x, k_y, z) = -\frac{\eta k}{2k_z} \begin{cases} (\tilde{\mathbf{J}} - (\tilde{\mathbf{J}} \cdot \hat{k}^-)\hat{k}^-)e^{jk_z z} & z < 0 \\ (\tilde{\mathbf{J}} - (\tilde{\mathbf{J}} \cdot \hat{k}^+)\hat{k}^+)e^{-jk_z z} & z > 0 \end{cases} \tag{14}$$

$$\tilde{\mathbf{H}}(k_x, k_y, z) = \frac{k}{2k_z} \cdot \begin{cases} \tilde{\mathbf{J}} \times \hat{k}^- e^{jk_z z} & z < 0 \\ \tilde{\mathbf{J}} \times \hat{k}^+ e^{-jk_z z} & z > 0 \end{cases}, \tag{15}$$

where

$$\begin{aligned} \hat{k}^- &= (k_x\hat{x} + k_y\hat{y} - k_z\hat{z})/k \\ \hat{k}^+ &= (k_x\hat{x} + k_y\hat{y} + k_z\hat{z})/k \,. \end{aligned} \tag{16}$$

The propagation constant in z direction is defined by $k_z^2 = k^2 - k_x^2 - k_y^2$ ($\mathrm{Im}\ k_z \le 0$), and k is the wave number in the considered medium. The H-field is discontinuous at $z = 0$ in such a way that $\tilde{\mathbf{J}} = \hat{z} \times (\tilde{\mathbf{H}}(z = 0^+) - \tilde{\mathbf{H}}(z = 0^-))$.

Cylindrical case. The electromagnetic field radiated by an electric current tube of radius ρ_s in the homogeneous space is given by

a) from $\tilde{J}_z(m, k_z)$

$$\begin{aligned} &\tilde{E}_z(\rho, m, k_z) \\ &= -\frac{\pi\eta}{2}\frac{k_\rho^2}{k}\rho_s \begin{cases} H_m^{(2)}(k_\rho\rho_s)J_m(k_\rho\rho)\ \tilde{J}_z & \rho \le \rho_s \\ J_m(k_\rho\rho_s)H_m^{(2)}(k_\rho\rho)\ \tilde{J}_z & \rho \ge \rho_s \end{cases} \end{aligned} \tag{17}$$

$$\tilde{H}_z(\rho, m, k_z) = 0 \tag{18}$$

b) from $\tilde{J}_\phi(m, k_z)$

$$\begin{aligned} &\tilde{E}_z(\rho, m, k_z) \\ &= \frac{\pi\eta}{2}\frac{mk_z}{k} \begin{cases} H_m^{(2)}(k_\rho\rho_s)J_m(k_\rho\rho)\ \tilde{J}_\phi & \rho \le \rho_s \\ J_m(k_\rho\rho_s)H_m^{(2)}(k_\rho\rho)\ \tilde{J}_\phi & \rho \ge \rho_s \end{cases} \end{aligned} \tag{19}$$

$$\begin{aligned} &\tilde{H}_z(\rho, m, k_z) \\ &= \frac{j\pi}{2}k_\rho\rho_s \begin{cases} H_m^{(2)'}(k_\rho\rho_s)J_m(k_\rho\rho)\ \tilde{J}_\phi & \rho < \rho_s \\ J_m'(k_\rho\rho_s)H_m^{(2)}(k_\rho\rho)\ \tilde{J}_\phi & \rho > \rho_s \,, \end{cases} \end{aligned} \tag{20}$$

where $k_\rho = \sqrt{k^2 - k_z^2}$. The other components of the electromagnetic field are calculated by using the following expressions

$$\tilde{E}_\phi = -\frac{mk_z}{k_\rho^2\rho}\,\tilde{E}_z + j\eta\frac{k}{k_\rho^2}\,\frac{\partial\tilde{H}_z}{\partial\rho} \tag{21}$$

$$\tilde{E}_\rho = -j\frac{k_z}{k_\rho^2}\,\frac{\partial\tilde{E}_z}{\partial\rho} - \eta\frac{mk}{k_\rho^2\rho}\,\tilde{H}_z \tag{22}$$

$$\tilde{H}_\phi = -j\frac{1}{\eta}\frac{k}{k_\rho^2}\,\frac{\partial\tilde{E}_z}{\partial\rho} - \frac{mk_z}{k_\rho^2\rho}\,\tilde{H}_z \tag{23}$$

$$\tilde{H}_\rho = \frac{1}{\eta}\frac{mk}{k_\rho^2\rho}\,\tilde{E}_z - j\frac{k_z}{k_\rho^2}\,\frac{\partial\tilde{H}_z}{\partial\rho}\,. \tag{24}$$

The fields caused by a ρ-directed electric current source J_ρ are evaluated by using transverse magnetic replacement current $\mathbf{M}^{rep}$

$$\tilde{\mathbf{M}}^{rep}(\rho, m, k_z) = \frac{\eta}{k}(\hat{\phi}k_z - \hat{z}\frac{m}{\rho})\tilde{J}_\rho\,. \tag{25}$$

This equation is simply to derive from the general replacement relation between electric and magnetic currents [25]

$$\mathbf{M}^{rep}(x,y,z) = \frac{j\eta}{k}\nabla \times \mathbf{J}(x,y,z)\ . \tag{26}$$

Spherical case. The electromagnetic field radiated by an electric current shell of radius r_s in the homogeneous space is given by ($\hat{J}_n$ and $\hat{H}_n^{(2)}$ denote Schelkunoff's spherical Bessel/Hankel functions [16])

a) from $\tilde{J}_\theta(m,n)$

$$\tilde{E}_\theta(r,n,m) = -\frac{\eta r_s}{r}\begin{cases}\hat{H}_n^{(2)'}(kr_s)\hat{J}_n'(kr)\ \tilde{J}_\theta & r \le r_s\\ \hat{J}_n'(kr_s)\hat{H}_n^{(2)'}(kr)\ \tilde{J}_\theta & r \ge r_s\end{cases} \tag{27}$$

$$\tilde{E}_r(r,n,m) = -\frac{\eta r_s}{kr^2}\sqrt{n(n+1)}\begin{cases}\hat{H}_n^{(2)'}(kr_s)\hat{J}_n(kr)\ \tilde{J}_\theta & r < r_s\\ \hat{J}_n'(kr_s)\hat{H}_n^{(2)}(kr)\ \tilde{J}_\theta & r > r_s\end{cases} \tag{28}$$

$$\tilde{H}_\phi(r,n,m) = \frac{jr_s}{r}\begin{cases}\hat{H}_n^{(2)'}(kr_s)\hat{J}_n(kr)\ \tilde{J}_\theta & r < r_s\\ \hat{J}_n'(kr_s)\hat{H}_n^{(2)}(kr)\ \tilde{J}_\theta & r > r_s\end{cases} \tag{29}$$

b) from $\tilde{J}_\phi(m,n)$

$$\tilde{E}_\phi(r,n,m) = -\frac{\eta r_s}{r}\begin{cases}\hat{H}_n^{(2)}(kr_s)\hat{J}_n(kr)\ \tilde{J}_\phi & r \le r_s\\ \hat{J}_n(kr_s)\hat{H}_n^{(2)}(kr)\ \tilde{J}_\phi & r \ge r_s\end{cases} \tag{30}$$

$$\tilde{H}_\theta(r,n,m) = \frac{jr_s}{r}\begin{cases}\hat{H}_n^{(2)}(kr_s)\hat{J}_n'(kr)\ \tilde{J}_\phi & r < r_s\\ \hat{J}_n(kr_s)\hat{H}_n^{(2)'}(kr)\ \tilde{J}_\phi & r > r_s\end{cases} \tag{31}$$

$$\tilde{H}_r(r,n,m) = \frac{jr_s}{kr^2}\sqrt{n(n+1)}\begin{cases}\hat{H}_n^{(2)}(kr_s)\hat{J}_n(kr)\ \tilde{J}_\phi & r \le r_s\\ \hat{J}_n(kr_s)\hat{H}_n^{(2)}(kr)\ \tilde{J}_\phi & r \ge r_s\ .\end{cases} \tag{32}$$

The fields caused by r-directed electric source J_r are evaluated by using transverse magnetic replacement source

$$\tilde{M}_\phi^{rep}(r,n,m) = \frac{j\eta}{k}\frac{1}{r}\sqrt{n(n+1)}\tilde{J}_r\ , \tag{33}$$

which can be derived from (26). Eq. (33) is valid if $J_r = 0$ for $\theta = 0^0$ and $\theta = 180^0$, or if the source has no ϕ dependence.

REFERENCES

[1] P-S. Kildal and J. Sanford, "Analysis of conformal antennas by using spectral domain techniques for curved structures," *Proc. of COST 245 - ESA workshop on active antennas*, Noordwijk, The Netherlands, 1996, pp. 17-26.

[2] D. M. Pozar, "Input impedance and mutual coupling of rectangular microstrip antennas," *IEEE Trans. Antennas Propagat.*, Vol. 30, pp. 1191-1196, Nov. 1982.

[3] R. Mittra, C. H. Chan, and T. Cwik, "Techniques for analyzing frequency selective surfaces - a review," *Proc. IEEE*, Vol. 76, pp. 1593-1615, Dec. 1988.

[4] N. K. Das and D. M. Pozar, "A generalized spectral-domain Green's function for multilayer dielectric substrates with application to multilayer transmission lines," *IEEE Trans. Microwave Theory Tech.*, Vol. 35, pp. 326-335, Mar. 1987.

[5] D. M. Pozar, "Radiation and scattering from a microstrip patch on a uniaxial substrate," *IEEE Trans. Antennas Propagat.*, Vol. 35, pp. 613-621, June 1987.

[6] J. R. Mosig, "Integral equation technique," in *Numerical techniques for microwave and millimeter-wave passive structures*, Ed. T. Itoh, Wiley, New York, 1989, pp. 133-213.

[7] A. Nakatani, N. G. Alexopoulos, "Microstrip elements on cylindrical substrates - general algorithm and numerical results," *Electromagnetics*, Vol. 9, pp. 405-426, 1989.

[8] W. C. Chew, *Waves and fields in inhomogeneous media*, IEEE Press, New York, 1995.

[9] T. Itoh and W. Menzel, "A full-wave analysis method for open microstrip structures," *IEEE Trans. Antennas Propagat.*, Vol. 29, pp. 63-68, Jan. 1981.

[10] K. A. Michalski, and J. R. Mosig, "Multilayered media Green's functions in integral equation formulations," *IEEE Trans. Antennas Propagat.*, Vol. 45, pp. 508-519, March 1997.

[11] M. Abramowitz and I. A. Stegun, *Handbook of mathematical functions*, Dover Publications, New York, 1972.

[12] W. Y. Tam and K. M. Luk, "Resonance in spherical-circular microstrip structures," *IEEE Trans. Microwave Theory Tech.*, Vol. 39, pp. 700-704, Apr. 1991.

[13] R. Leijon, "Radiation from mobile phone antennas close to the human body," Technical Report No. 270L, Department of Microwave Technology, Chalmers University of Technology, Gothenburg, Aug. 1997.

[14] P.-S. Kildal, A.A. Kishk, and Z. Šipuš, "Asymptotic boundary conditions for strip-loaded and corrugated surfaces," *Microwave Opt. Technol. Lett.*, Vol. 14, pp. 99-101, Feb 1997.

[15] A. A. Kishk, P-S. Kildal, G. Manara, and A. Monorchio, "An asymptotic boundary condition for corrugated surfaces and its application to calculate scattering from circular cylinders with dielectric filled corrugations," Submitted to *IEE Proceedings - Microw. Antennas Propagat.*

[16] R. F. Harrington, *Time-harmonic electromagnetic fields*, McGraw-Hill, New York, 1961.

[17] A. A. Kishk, P-S. Kildal, "Asymptotic boundary conditions for strip-loaded scatters applied to cylinders under oblique incidence," *IEEE Trans. Antennas Propagat.*, Vol. 45, pp. 51-56, Jan. 1997.

[18] Z. Šipuš, H. Merkel, and P-S. Kildal, "Green's functions for planar soft and hard surfaces derived by asymptotic boundary conditions," Accepted for publication in *IEE Proceedings - Microw. Antennas Propagat.*

[19] W. Y. Tam, A. K. Y. Lai, and K. M. Luk, "Mutual coupling between cylindrical rectangular microstrip antennas," *IEEE Trans. Antennas Propagat.*, Vol. 43, pp. 897-899, Aug. 1995.

[20] E. H. Newman and D. Forrai, "Scattering from a microstrip patch," *IEEE Trans. Antennas Propagat.*, Vol. 35, pp. 245-251, Mar. 1987.

[21] N. Herscovici, Z. Šipuš, P-S. Kildal, "The cylindrical omnidirectional patch antenna," *Proc. of IEEE AP-S Symposium*, Montreal, 1997, pp. 924-927.

[22] T. K. Wu, "Fast convergent integral equation solution of strip gratings on dielectric substrate," *IEEE Trans. Antennas Propagat.*, Vol. 35, pp. 205-207, Feb. 1987.

[23] P-S. Kildal, A. A. Kishk, and A. Tengs, "Reduction of forward scattering from cylindrical objects using hard surfaces," *IEEE Trans. Antennas Propagat.*, pp. 1509-1520, Nov. 1996.
[24] G. Manara, G. Pelosi, A. Monorchio, and R. Coccioli, "Plane-wave scattering from cylinders with transverse corrugations," *Electron. Lett.*, Vol. 31, pp. 437-438, 1995.
[25] L. B. Felsen and N. Marcuvitz, *Radiation and scattering of waves*, Prentice-Hall, New Jersey, 1973.